# Flexible General Branch Model Unified Power Flow Algorithm for Future Flexible AC/DC Networks

Abraham Alvarez Bustos and Behzad Kazemtabrizi
*Engineering Department*
*Durham University*
Durham, United Kingdom
abraham.alvarez-bustos@durham.ac.uk
behzad.kazemtabrizi@durham.ac.uk

***Abstract*—This paper presents a new Flexible General Branch Model (FGBM) for the power flow solution of hybrid AC/DC grids. The model is an improvement of MATPOWER's original branch model, by incorporating extra degrees of freedom in form of additional state variables to model both conventional AC branches as well as different types of AC/DC interface devices such as Voltage Source Converters (VSC). A detailed description of the proposed flexible model is shown. Furthermore, the model is used in a new unified power flow algorithm based on the Newton Raphson method. This algorithm is also an extension of the already powerful one employed in MATPOWER. Due to the nature of the developed model, there is no need of identifying or differentiate between AC, DC or even VSC nodes. As a result, all power flow calculations are obtained with the traditional NR method. Power and Voltage Control variables are created for all the modelled elements that requires them. Necessary modifications to the original MATPOWER's power flow algorithm to include them are developed and described. Finally, detailed simulations validate the algorithm and model's accuracy.**

***Index Terms*—AC/DC, HVDC transmission, VSC, Power flow analysis, VSC Power Control, Voltage Control, MATPOWER.**

## I. Introduction

Throughout the last fifteen years, Power Systems have been going through a series of significant transformations. With the rising levels of large-scale renewable resources penetration, which have inherently more variability in their outputs than conventional resources, there is a need for accommodating a higher degree of flexibility for power flow transmission across the grid. This scenario has led to the creation of hybrid AC/DC Supergrids [1]. They not only inlude Phase-shifting transformers (PSTs) and flexible AC transmission systems (FACTS), but also, their key component, the Voltage Source Converter (VSC)-based HVDC system. The latter offers independent control of active and reactive power, greater flexibility for operation and easier expandability to multi-terminal DC (MTDC) configurations [2].

In Europe, the notion of Supergrid has been proposed to make sufficient use of its potential rich offshore wind power and multiple interconnections. However, in highly meshed networks like the European one, several power flow control devices are deployed [2]. Therefore, analysis of the effects of their mutual interaction is imperative, otherwise Transmission System Operators (TSO) will face the risk that these devices will not realise their full potential. Moreover, they could even contribute to unwanted system behaviours [3]. Consecuently, numerous studies of VSC-based MTDC grids have been done, such as Stability Analysis, Optimal Power Flow (OPF) and Voltage Droop Control (VDC) [4]–[6].

The main core of the aforementioned analysis is the Hybrid AC/DC Power Flow. Two different strategies have been suggested for the solution of their non-linear equations, namely the Sequential and the Unified Power Flow. While in the unified approach, the AC and DC equations are solved at the same time, in the sequential approach, the AC and DC systems are solved in a successive fashion [7], [8].

The sequential power flow for hybrid networks with VSC approach was studied in [9]–[11]. Whereas [10] neglects the VSC lossless and fixed control parameters, in [9] and [11] converter losses, filters and slack bus control are considered. A sequential power flow algorithm has been proposed as an addition to MATPOWER in [11].

On the other hand, the unified method algorithm, describing an application of an VSC-HVDC link, was first reported in [12]. Then, [13] proposed an improvement of the unified algorithm including control and losses in the VSC. The inclusion of constrained load flow in the unified power flow algorithm including VSC was reported in [8].

Even though sequential methods can be added as an extension of existing Power flow software, the convergence of the internal loop affects the convergence of the external one, creating divergence problems. Such high number of iterative loops makes the algorithm slow. Moreover their first order convergence feature reduces calculations accuracy. On the other hand, unified power flow considers high precision quadratic convergence. Furthermore, it is considerably faster by avoiding internal loops to solve the grid [8], [14].

In all previously mentioned power flow algorithms, conventional VSC model has been used. In [15] a new model of VSC for unified power flow algorithms has been introduced, where the VSC is modelled as a combination of complex tap transformers with a variable shunt susceptance. Due to similarity between this new VSC model and the traditional

Abraham Alvarez Bustos is sponsored by Consejo Nacional de Ciencia y Tecnología (CONACyT) and Secretaría de Energía (SENER), México

modelling of the power grid an opportunity to develop a flexible AC/DC branch model has been opened.

This paper therefore presents a new Flexible General Branch Model for power flow solution of AC/DC grids. It can be used to seamlessly model conventional AC branches, Controlled Tap Transformers (CTT), PST and VSC. Due to high versatility and nature of the developed model, no differentiation between the AC and DC grid is necessary. Thus, traditional AC power flow equations can be used to solve AC/DC grids. In order to preform full power and voltage control, extra state variables are added to the traditional Jacobian. Thus, the new proposed Flexible AC/DC Power Flow algorithm (FPFA) will maintain all the advantages of the unified power flow in a simpler version of it.

The reminder of this paper is as follows: Section II introduces the new Flexible General Branch Model (FGBM) as an extension to MATPOWER's branch model by modelling a variety of control devices, including VSC. Section III introduces various modes of control for FGBM and VSC's asserting a high degree of flexibility in the model. Section IV presents the new FPFA for solving hybrid AC/DC networks modelled via the FGBM. Finally simulation case studies for a modified IEEE test system are presented in Section V, followed by simulation discussion and conclusion in Sections VI, and VII.

## II. New Flexible AC/DC General Branch Model

The original General Branch Model used in MATPOWER has proven to be effective for power flow analysis. Original branch model can be found in [16]. The combination of this one with the VSC model developed in [15] will transform the original model from an already powerful AC branch model to the next generation Flexible AC/DC General Branch Model (FGBM) that the new power flow analysis tools need to adequately simulate the future AC/DC grid. The proposed model is shown in Fig. 1.

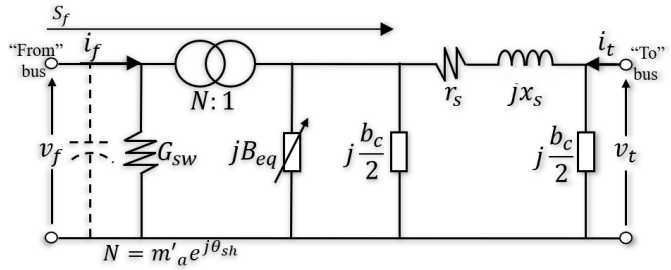


Fig. 1. Flexible AC/DC General Branch Model

There are five key components of this FGBM model. The central one is a complex tap transformer, shown in (1). This one has two control variables, $m_a$ and $\theta_{sh}$. While the $\theta_{sh}$ will be controlling the amount of real power to be transmitted, the $m_a$ of the ideal tap-changing transformer corresponds to the VSC's amplitude modulation coefficient. The $k_2$ constant will vary depending on the type of element to be modelled [17].

$$N = m'_a e^{j\theta_{\text{sh}}} = k_2 m_a e^{j\theta_{\text{sh}}} \tag{1}$$

Secondly, a variable susceptance $jB_{eq}$ is included in order to compensate the reactive power balance equation by absorbing or supplying reactive power at the AC terminals of VSC's (when modelling VSC's). This susceptance essentially represents the reactive power control capabilities of the actual VSC. Thus, in case of modelling VSC-HVDC links using the FGBM, the reactive power flow through the DC link remains zero throughout the solution process. Thirdly, there are complementary elements within the FGBM to represent a variety of elements when applicable, e.g. When modelling a VSC, the inductive reactance $jx_s$ and the series resistance $r_s$, within the full $\pi$ transmission line model, can be used to model the interface magnetics and the ohmic losses respectively. In contrast to, the FGBM can also be simply used to represent conventional AC branches simply by setting the appropriate parameters within the $\pi$ section. Finally, the shunt conductance $G_{sw}$ relates to the VSC switching losses. Under nominal values of voltage and current, these losses are constant, generating a constant loss $G_0$. However, even though the voltage remains practically constant, the load current will vary according to the prevailing operating condition. Hence, $G_{sw}$ will be corrected by the quadratic ratio of the actual current over the nominal current as shown in (2) [15].

$$G_{sw} = G_0 \left( \frac{{i_f}^{act}}{{i_f}^{nom}} \right)^2 \tag{2}$$

### A. Flexible General Model Equations

The 2x2 admittance matrix $Y_{br}$ for the FGBM is expressed in terms of the current injections, $i_f$ and $i_t$, and the respective terminal voltages, $v_f$ and $v_t$ as shown below in (3). It is worth highlighting that even though, when modelling a VSC, the $v_f$ and $v_t$ will be the DC voltage $v_{dc}$ and the AC voltage $v_{ac}$ respectively, there is no need to differentiate between AC and DC nodes. The branch admittance matrix for the FBGM is shown in (4).

$$\begin{bmatrix} i_f \\ i_t \end{bmatrix} = \begin{bmatrix} y_{ff} & y_{ft} \\ y_{tf} & y_{tt} \end{bmatrix} \begin{bmatrix} v_f \\ v_t \end{bmatrix} = \begin{bmatrix} Y_{br} \end{bmatrix} \begin{bmatrix} v_f \\ v_t \end{bmatrix} \tag{3}$$

$$\mathbf{Y_{br}} = \begin{bmatrix} G_{sw} + (y_s + j\frac{b_c}{2} + jB_{eq})\frac{1}{{m'_a}^2} & \frac{-y_s}{m'_a e^{-j\theta_{\text{sh}}}} \\ \frac{-y_s}{m'_a e^{j\theta_{\text{sh}}}} & y_s + j\frac{b_c}{2} \end{bmatrix} \tag{4}$$

Finally, the selection of the desired element to be modelled is done by setting certain parameters to configure the FGBM appropriately as shown in Table I. For example, for modelling a two-level VSC the parameter $k_2$ is configured to have a value of $\sqrt{3}/2$.

## III. VSC and FGBM Control

### A. VSC Control

Flexibility of VSC operation and control is indeed the landmark of future hybrid AC/DC grids. As a result, proper

TABLE I
VALUES FOR THE DESIRED MODEL

| Parameter | Branches | CTT | PST | VSC |
|---|---|---|---|---|
| $G_{sw}$ | 0 | 0 | 0 | $*^a$ |
| $B_{eq}$ | 0 | 0 | 0 | $*^a$ |
| $\theta_{sh}$ | 0 | 0 | $*^a$ | $*^a$ |
| $k_2$ | 1 | 1 | 1 | $*^a$ |
| $m_a$ | 1 | $*^a$ | 1 | $*^a$ |
| $b_c$ | $*^a$ | 0 | 0 | 0 |
| $r_s$ | $*^a$ | $*^a$ | $*^a$ | $*^a$ |
| $x_s$ | $*^a$ | $*^a$ | $*^a$ | $*^a$ |

$*^a$ : Element parameter

representation of VSC control charactersitics is paramount for the adequate simulation of flexible AC/DC transmission networks. In practice VSC's have different control modes as shown in Table II [8], [9].

TABLE II
VSC CONTROL MODES

| Control Mode | Constraint 1 | Constraint 2 | VSC Control Type |
|---|---|---|---|
| 1 | $\theta_{sh}$ | $v_{ac}$ | I |
| 2 | $P_f$ | $Q_{ac}$ | |
| 3 | $P_f$ | $v_{ac}$ | |
| 4 | $v_{dc}$ | $Q_{ac}$ | II |
| 5 | $v_{dc}$ | $v_{ac}$ | |
| 6 | $v_{dc}$ droop | $Q_{ac}$ | III |
| 7 | $v_{dc}$ droop | $v_{ac}$ | |

It can be noticed that each VSC control mode has two constraints for either maintaining constant power or constant voltage or a combination of them. This can create resolvability problems if there is not a suitable selection on the converter control mode to be used on a DC grid or link. Therefore, from modelling perspective there may be more than one type of VSC present within a system depending on the control requriements. E.g, when modelling a DC link or grid, not only there must be at least one converter type #II or #III but also there must not be more than one of them to control DC voltage. Additionally, all the remaining converters must be type #I. Moreover, type #I converter must be used if using the converter to connect a wind farm, a photovoltaic power plant, energy storage devices or pasive networks [8], [18]. By following these rules a window for a feasible solution of the grid will be opened.

### B. FGBM Control

Due to FGBM design for transparent resolvability of AC/DC hybrid grids, converter types work as converter identifiers to meet a "Zero Constraint" for the connected DC grids. Converters type #I will use the suceptance $B_{eq}$ to absorb or supply reactive power so that only active power flows through the DC grid. Thus, reactive powers are always zero. Converters type #II do not need to meet the zero constraint since the reactive power flowing through them will become zero naturally by restricting the reactive powers in converters type #I.

As an advantage, the FGBM is designed to tackle each one of the aforementioned constraints individually by modifying the value of a specific variable. Consequently, the model is not limited by the VSC control modes. Moreover, in order to simulate realistically the power grid, it has the option to activate or deactivate the desired control over the modelled element to whatever suits better. Table III summarises this relation.

TABLE III
VARIABLE - CONSTRAINT RELATION

| Variable | Control |
|---|---|
| $\theta_{sh}$ | $\theta_{sh}$ |
| $\theta_{sh}$ | $P_f$ |
| $m_a$ | $v_t$ |
| $m_a$ | $Q_t$ |
| $B_{eq}$ | $v_{dc}$ |
| $B_{eq}$ | $Zero\ Constraint$ |

Up to this point, by using tables I and III, it can be appreciated that the model is able to simulate either a branch, CTT, PST, or VSC if the correct values for each variable in (4) are selected. Is worth noticing that, even with traditional unmodified power flow calculation, hybrid AC/DC grids can still be simulated if this new FGBM is implemented and the parameters of $B_{eq}$ to meet the zero constraint are known. However, traditional Power Flow Analysis does not include $N$ as a variable of power flow control. Typically, the active power flow is controlled by setting a fixed Shift Angle value, $\theta_{\text{sh}}$. On the other hand, the voltage is controlled by setting a fixed tap in the transformer. Unfortunately, neither the relationship between shift angle and active power control, nor that between transformer tap and reactive power control, is linear. Any modifications to the set dispatch will result in a change in power through the FGBM. Furthermore, for the VSC, the value of the equivalent susceptance $B_{eq}$ must be calculated for each scenario too, so that the reactive power flowing through the DC side will always meet the zero constraint. As a consequence, for a full controllable and flexible power flow algorithm, new state variables and mismatch equations for these controllers need to be added to the Jacobian when solving by Newton's Method.

## IV. FLEXIBLE POWER FLOW ALGORITHM

In traditional Power Flow Analysis, the nodal bus injections are matched to the loads and generators injections to form the nodal power balance equations, expressed as a function of the complex bus voltages, where the voltage angle $V_a$ and the $V_m$ are the state variables [16]. Newton's Method is used to solve these the non-linear power balance equations [19], [20].

### A. Extended Mismatch Equations

In order to solve power flows considering full control over the FGBM, the system of non-linear mismatch equations $\mathbf{g}(\mathbf{X})$ is expanded as showed in (5).

$$\mathbf{g}(\mathbf{X}) = \begin{bmatrix} \mathbf{g_P^{\{i\}}}(\mathbf{X}) = 0 \\ \mathbf{g_Q^{\{i\}}}(\mathbf{X}) = 0 \\ \mathbf{g_{sh}^{\{i\}}}(\mathbf{X}) = 0 \\ \mathbf{g_{Qz}^{\{i\}}}(\mathbf{X}) = 0 \\ \mathbf{g_{Vf}^{\{i\}}}(\mathbf{X}) = 0 \\ \mathbf{g_{Vt}^{\{i\}}}(\mathbf{X}) = 0 \\ \mathbf{g_{Qt}^{\{i\}}}(\mathbf{X}) = 0 \end{bmatrix}, \mathbf{X} = \begin{bmatrix} \mathbf{V_a^{\{i\}}} & \forall i \in \mathcal{I}_{pv} \cup \mathcal{I}_{pq} \\ \mathbf{V_m^{\{i\}}} & \forall i \in \mathcal{I}_{pq} \\ \theta_{\text{sh}}^{\{i\}} & \forall i \in \mathcal{I}_{sh} \\ \mathbf{B_{eq}^{\{i\}}} & \forall i \in \mathcal{I}_{Qz} \\ \mathbf{m_a^{\{i\}}} & \forall i \in \mathcal{I}_{V_f} \\ \mathbf{m_a^{\{i\}}} & \forall i \in \mathcal{I}_{V_t} \\ \mathbf{B_{eq}^{\{i\}}} & \forall i \in \mathcal{I}_{Q_t} \end{bmatrix} \quad (5)$$

Where the vector $\mathbf{X}$ represent the state variables. Additionally, the sets of bus indices $\mathcal{I}_{ref}, \mathcal{I}_{pv}, \mathcal{I}_{pq}$ denote the reference, PV and PQ buses, respectively, whereas the indices $\mathcal{I}_{sh}$, $\mathcal{I}_{Qz}$, $\mathcal{I}_{V_f}$, $\mathcal{I}_{V_t}$, $\mathcal{I}_{Q_t}$, indicate the elements for active power control, zero constraint control, $V_f$ control nodes, $V_t$ control nodes and $Q_t$ control elements.

For a a specified pattern of load $S_d$ and generation $S_g$ per bus, the complex power balance equations of the system are calculated as:

$$\mathbf{g_s}(\mathbf{X}) = \mathbf{S_{bus}}(\mathbf{X}) + \mathbf{S_d} - \mathbf{S_g} = \mathbf{0} \quad (6)$$

$$\text{Where,} \quad \mathbf{S_{bus}}(\mathbf{X}) = [\mathbf{V}]\mathbf{I_{bus}}^* = [\mathbf{V}]\mathbf{Y_{bus}}^*\mathbf{V}^* \quad (7)$$

Also, for the complex power injections:

$$\mathbf{S_f^{\{i\}}} = \mathbf{C_f}[\mathbf{V}][\mathbf{Y_f^{\{i\}}}\mathbf{V}]^* \quad (8)$$

$$\mathbf{S_t^{\{i\}}} = \mathbf{C_t}[\mathbf{V}][\mathbf{Y_t^{\{i\}}}\mathbf{V}]^* \quad (9)$$

$$\text{Where,} \quad \mathbf{Y_f^{\{i\}}} = [\mathbf{Y_{ff}^{\{i\}}}]\mathbf{C_f} + [\mathbf{Y_{ft}^{\{i\}}}]\mathbf{C_t} \quad (10)$$

$$\text{And,} \quad \mathbf{Y_t^{\{i\}}} = [\mathbf{Y_{tf}^{\{i\}}}]\mathbf{C_f} + [\mathbf{Y_{tt}^{\{i\}}}]\mathbf{C_t} \quad (11)$$

Considering (6) to (11), the full detailed set of non-linear mismatch functions is described below in (12) to (18).

$$\mathbf{g_P^{\{i\}}}(\mathbf{X}) = Real(\mathbf{g_s^{\{i\}}}(\mathbf{X})) = 0 \quad (12)$$

$$\mathbf{g_Q^{\{i\}}}(\mathbf{X}) = Imag(\mathbf{g_s^{\{i\}}}(\mathbf{X})) = 0 \quad (13)$$

$$\mathbf{g_{sh}^{\{i\}}}(\mathbf{X}) = Real(\mathbf{S_f^{\{i\}}}(\mathbf{X})) - \mathbf{P_f^{\{i\}\,set}} = 0 \quad (14)$$

$$\mathbf{g_{Qz}^{\{i\}}}(\mathbf{X}) = Imag(\mathbf{S_f^{\{i\}}}(\mathbf{X})) = 0 \quad (15)$$

$$\mathbf{g_{V_f}^{\{i\}}}(\mathbf{X}) = Imag(\mathbf{g_s^{\{i\}}}(\mathbf{X})) = 0 \quad (16)$$

$$\mathbf{g_{V_t}^{\{i\}}}(\mathbf{X}) = Imag(\mathbf{g_s^{\{i\}}}(\mathbf{X})) = 0 \quad (17)$$

$$\mathbf{g_{Q_t}^{\{i\}}}(\mathbf{X}) = Imag(\mathbf{S_t^{\{i\}}}(\mathbf{X})) - \mathbf{Q_t^{\{i\}\,set}} = 0 \quad (18)$$

Where, $\mathbf{P_f^{\{i\}\,set}}$, and $\mathbf{Q_t^{\{i\}\,set}}$ are the desired active and reactive power control reference setting. For voltage control, $\mathcal{I}_{V_f}$ and $\mathcal{I}_{V_t}$ nodes are set as PV nodes, as a result, they are not included in the $\mathbf{g_Q^{\{i\}}}(\mathbf{X})$ power balance equation. Therefore, their reactive balance equations are considered in $\mathbf{g_{V_f}^{\{i\}}}(\mathbf{X})$ and $\mathbf{g_{V_t}^{\{i\}}}(\mathbf{X})$ with a constant voltage, and variable $B_{eq}$ and $m_a$ respectively.

### *B. NR Method and Extended Jacobian*

According to Newtons Method, the vector of state variables $\mathbf{X}$ can be approximated by performing Taylor series expansion of $\mathbf{g}(\mathbf{X})$ in which higher order terms can be neglected. Thus the iterative corrections are calculated as:

$$\Delta\mathbf{X} = -\mathbf{g}(\mathbf{X}) \cdot \mathbf{J^{-1}} \quad (19)$$

Jacobian matrix $\mathbf{J}$ represents the first order partial derivatives with respect to $\mathbf{X}$. Full Jacobian structure is shown in (20).

$$\begin{bmatrix} \Delta\mathbf{V_a^{\{i\}}} \\ \Delta\mathbf{V_m^{\{i\}}} \\ \Delta\theta_{\text{sh}}^{\{i\}} \\ \Delta\mathbf{B_{eq}^{\{i\}}} \\ \Delta\mathbf{m_a^{\{i\}}} \\ \Delta\mathbf{m_a^{\{i\}}} \\ \Delta\mathbf{B_{eq}^{\{i\}}} \end{bmatrix} = - \begin{bmatrix} \mathbf{g_P^{\{i\}}}(\mathbf{X}) \\ \mathbf{g_Q^{\{i\}}}(\mathbf{X}) \\ \mathbf{g_{sh}^{\{i\}}}(\mathbf{X}) \\ \mathbf{g_{Qz}^{\{i\}}}(\mathbf{X}) \\ \mathbf{g_{Vf}^{\{i\}}}(\mathbf{X}) \\ \mathbf{g_{Vt}^{\{i\}}}(\mathbf{X}) \\ \mathbf{g_{Qt}^{\{i\}}}(\mathbf{X}) \end{bmatrix} /$$

$$\begin{bmatrix} \frac{\partial \mathbf{g_P}}{\partial \mathbf{V_a}} & \frac{\partial \mathbf{g_P}}{\partial \mathbf{V_m}} & \frac{\partial \mathbf{g_P}}{\partial \theta_{\text{sh}}} & \frac{\partial \mathbf{g_P}}{\partial \mathbf{B_{eq}}} & \frac{\partial \mathbf{g_P}}{\partial \mathbf{m_a}} & \frac{\partial \mathbf{g_P}}{\partial \mathbf{m_a}} & \frac{\partial \mathbf{g_P}}{\partial \mathbf{B_{eq}}} \\ \frac{\partial \mathbf{g_Q}}{\partial \mathbf{V_a}} & \frac{\partial \mathbf{g_Q}}{\partial \mathbf{V_m}} & \frac{\partial \mathbf{g_Q}}{\partial \theta_{\text{sh}}} & \frac{\partial \mathbf{g_Q}}{\partial \mathbf{B_{eq}}} & \frac{\partial \mathbf{g_Q}}{\partial \mathbf{m_a}} & \frac{\partial \mathbf{g_Q}}{\partial \mathbf{m_a}} & \frac{\partial \mathbf{g_Q}}{\partial \mathbf{B_{eq}}} \\ \frac{\partial \mathbf{g_{sh}}}{\partial \mathbf{V_a}} & \frac{\partial \mathbf{g_{sh}}}{\partial \mathbf{V_m}} & \frac{\partial \mathbf{g_{sh}}}{\partial \theta_{\text{sh}}} & \frac{\partial \mathbf{g_{sh}}}{\partial \mathbf{B_{eq}}} & \frac{\partial \mathbf{g_{sh}}}{\partial \mathbf{m_a}} & \frac{\partial \mathbf{g_{sh}}}{\partial \mathbf{m_a}} & \frac{\partial \mathbf{g_{sh}}}{\partial \mathbf{B_{eq}}} \\ \frac{\partial \mathbf{g_{Qz}}}{\partial \mathbf{V_a}} & \frac{\partial \mathbf{g_{Qz}}}{\partial \mathbf{V_m}} & \frac{\partial \mathbf{g_{Qz}}}{\partial \theta_{\text{sh}}} & \frac{\partial \mathbf{g_{Qz}}}{\partial \mathbf{B_{eq}}} & \frac{\partial \mathbf{g_{Qz}}}{\partial \mathbf{m_a}} & \frac{\partial \mathbf{g_{Qz}}}{\partial \mathbf{m_a}} & \frac{\partial \mathbf{g_{Qz}}}{\partial \mathbf{B_{eq}}} \\ \frac{\partial \mathbf{g_{V_f}}}{\partial \mathbf{V_a}} & \frac{\partial \mathbf{g_{V_f}}}{\partial \mathbf{V_m}} & \frac{\partial \mathbf{g_{V_f}}}{\partial \theta_{\text{sh}}} & \frac{\partial \mathbf{g_{V_f}}}{\partial \mathbf{B_{eq}}} & \frac{\partial \mathbf{g_{V_f}}}{\partial \mathbf{m_a}} & \frac{\partial \mathbf{g_{V_f}}}{\partial \mathbf{m_a}} & \frac{\partial \mathbf{g_{V_f}}}{\partial \mathbf{B_{eq}}} \\ \frac{\partial \mathbf{g_{V_t}}}{\partial \mathbf{V_a}} & \frac{\partial \mathbf{g_{V_t}}}{\partial \mathbf{V_m}} & \frac{\partial \mathbf{g_{V_t}}}{\partial \theta_{\text{sh}}} & \frac{\partial \mathbf{g_{V_t}}}{\partial \mathbf{B_{eq}}} & \frac{\partial \mathbf{g_{V_t}}}{\partial \mathbf{m_a}} & \frac{\partial \mathbf{g_{V_t}}}{\partial \mathbf{m_a}} & \frac{\partial \mathbf{g_{V_t}}}{\partial \mathbf{B_{eq}}} \\ \frac{\partial \mathbf{g_{Q_t}}}{\partial \mathbf{V_a}} & \frac{\partial \mathbf{g_{Q_t}}}{\partial \mathbf{V_m}} & \frac{\partial \mathbf{g_{Q_t}}}{\partial \theta_{\text{sh}}} & \frac{\partial \mathbf{g_{Q_t}}}{\partial \mathbf{B_{eq}}} & \frac{\partial \mathbf{g_{Q_t}}}{\partial \mathbf{m_a}} & \frac{\partial \mathbf{g_{Q_t}}}{\partial \mathbf{m_a}} & \frac{\partial \mathbf{g_{Q_t}}}{\partial \mathbf{B_{eq}}} \end{bmatrix} \quad (20)$$

The new non linear equation system presented in (20) will be solved iteratively until a set tolerance $\epsilon$ is reached. FPFA flowchart for the FGBM is showed in Fig. 2.

## V. Case Study and Simulations

This section presents the simulation of the proposed FPFA algorithm with the implementation of the FGBM for the solution of hybrid AC/DC grids. The Algorithm is an improvement to the original MATPOWER code. In order to verify accuracy of the model and algorithm, the simulation is preformed in the same test system reported in [8], where a comparison against the sequential method presented in [9] and the unified method presented in [8] is reported. Notice that both in [9] as well as in [8], the most basic general model of a VSC station is is used, which is represented by a controllable voltage source behind the phase reactor with a complex impedance. The power flow algorithm is set within the tolerance shown in (21).

$$\epsilon = 1e10^{-12} \quad (21)$$

The test system case consists of two asynchronous AC grids interconnected trough two MTDC grids. The AC grid #1 was the IEEE 57 bus system consisting of 7 generators, 80 transmission lines and 42 loads. On the other hand, the

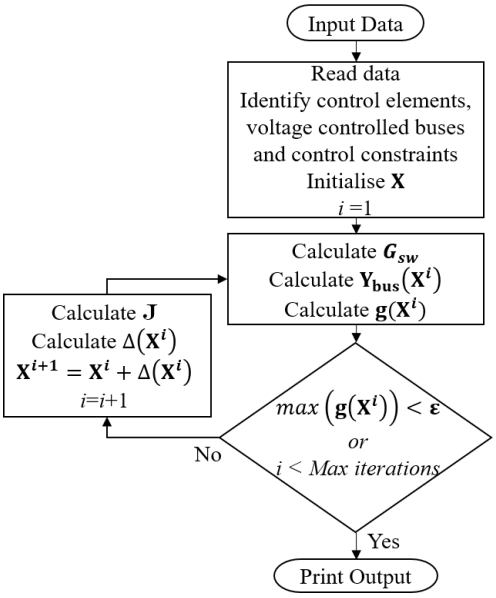


Fig. 2. Flexible Power Flow Algorithm Flowchart

AC grid #2 was the IEEE 14 bus system, supplying 11 loads through 20 lines with 5 generators. While, DC grid #1 consists in 3 DC buses connected with a ring topology of DC lines and 3 VSC for the AC/DC link, DC grid #2 consists in 7 bipolar buses, where 5 were connected to a VSC and 2 were pure DC buses. Bus 9 had a 30 MVA generator and a pure DC load of 10 MW. Figure 3 shows the combined test system diagram.

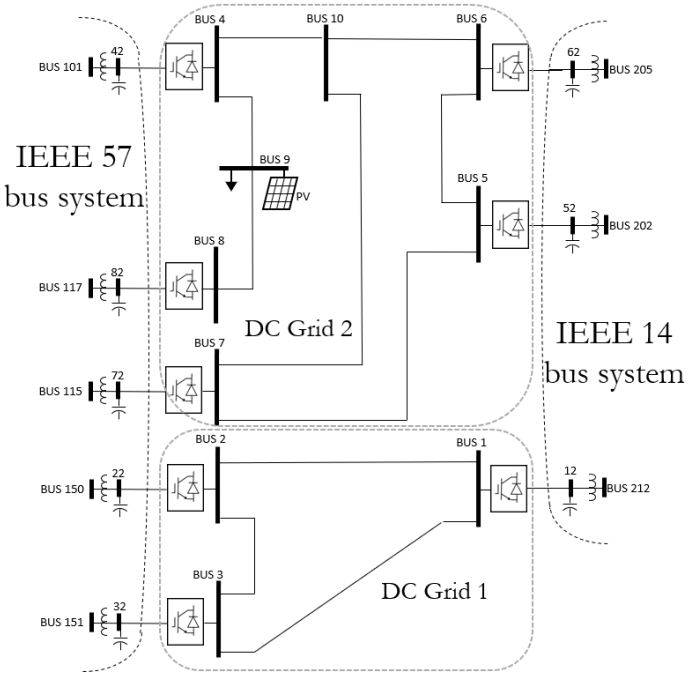


Fig. 3. IEEE 57 - IEEE 14 MTDC Link

DC grid parameters can be found in [8]. VSCs parameters are given in Table IV. VSC control settings are presented in Table V. Notice that for active power control, in each DC area at least one VSC has to remain as free to include the active power loss though the DC lines.

TABLE IV
VSC PARAMETERS

| VSC No. | Capacity $S_n$ [pu] | Transformer $Z_{tr}$ [pu] | Filter $B_f$ [pu] | Reactor $Z_s$ [pu] | Loss $G_0$ [pu] |
|---|---|---|---|---|---|
| 1 | 2 | 0.0010+j0.0033 | 0 | 0.05 | 0.001 |
| 2,3 | 1 | 0.0015+j0.0500 | 0 | 0.075 | 0.002 |
| 4 | 2 | 0.0010+j0.0033 | 0 | 0.05 | 0.001 |
| 5,6,7,8 | 1 | 0.0015+j0.0500 | 0 | 0.075 | 0.002 |

TABLE V
VSC SET CONTROL

| DC Grid | VSC No. | Control Mode | Zero Constraint | $V_{dc}$ [pu] | $P_f$ [MW] | $V_t$ [pu] | $Q_t$ [MVAr] |
|---|---|---|---|---|---|---|---|
| 1 | 1 | 5 | Free | 1 | *** | 1.06 | *** |
| | 2 | 3 | Active | *** | -50 | 0.99 | *** |
| | 3 | 3 | Active | *** | -50 | 1.03 | *** |
| 2 | 4 | 4 | Free | 0.995 | *** | *** | 0 |
| | 5 | 2 | Active | *** | -50 | *** | 0 |
| | 6 | 2 | Active | *** | -50 | *** | 10 |
| | 7 | 3 | Active | *** | 90 | 1.001 | *** |
| | 8 | 3 | Active | *** | -60 | 1 | *** |

## VI. SIMULATION RESULTS AND DISCUSSION

Tables VI and VII summarize the AC and DC active and reactive powers and voltages of the VSC converters, and elements connected to the 2 MTDC grids and their respective AC nodes for the link.

TABLE VI
VSC POWER FLOW CONTROL RESULTS

| From bus | To bus | $P_f$ [Mw] | $P_t$ [Mw] | $Q_f$ [MVAr] | $Q_t$ [MVAr] | $m_a$ [pu] | $\theta_{sh}$ [Degrees] |
|---|---|---|---|---|---|---|---|
| 1 | 2 | -62.08 | 62.47 | 0 | 0 | 1 | 0 |
| 2 | 3 | -12.47 | 12.48 | 0 | 0 | 1 | 0 |
| 3 | 1 | 37.52 | -37.24 | 0 | 0 | 1 | 0 |
| 1 | 212 | 99.32 | -93.59 | 0 | 46.3 | 0.748 | 0 |
| 2 | 150 | -50 | 52.21 | 0 | -8.5 | 0.861 | 27.331 |
| 3 | 151 | -50 | 51.97 | 0 | 1.3 | 0.83 | 25.328 |
| 4 | 9 | -78.84 | 79.47 | 0 | 0 | 1 | 0 |
| 4 | 10 | -9.14 | 9.15 | 0 | 0 | 1 | 0 |
| 5 | 6 | -6.57 | 6.57 | 0 | 0 | 1 | 0 |
| 5 | 7 | 56.57 | -56.08 | 0 | 0 | 1 | 0 |
| 6 | 10 | 43.43 | -43.24 | 0 | 0 | 1 | 0 |
| 7 | 10 | -33.92 | 34.09 | 0 | 0 | 1 | 0 |
| 8 | 9 | 60 | -59.47 | 0 | 0 | 1 | 0 |
| 4 | 101 | 87.99 | -84.04 | 0 | 0 | 0.751 | 0 |
| 5 | 202 | -50 | 51.91 | 0 | 0 | 0.81 | 8.546 |
| 6 | 205 | -50 | 52.1 | 0 | 10 | 0.837 | 10.833 |
| 7 | 115 | 90 | -82.9 | 0 | -48.2 | 0.743 | 9.009 |
| 8 | 117 | -60 | 63.1 | 0 | 4.66 | 0.87 | 12.006 |

Reactive injection to the DC grid by the VSC type #I shows that the zero constraint has been achieved. It is noticeable that active power has been fully controlled by both MTDC. Furthermore, the value of $\theta_{sh}$ has been obtained for all active power controlled elements. The algorithm has calculated successfully the modulation coefficient and the required value of

TABLE VII
VOLTAGE MAGNITUDE AND ANGLE RESULTS

| Bus | $V_m$ | $V_a$ | Bus | $V_m$ | $V_a$ |
|---|---|---|---|---|---|
| 1 | 1 | 3.765 | 101 | 1.04 | 0.000 |
| 2 | 1.006 | 3.765 | 115 | 1.001 | -7.837 |
| 3 | 1.007 | 3.765 | 117 | 1 | -8.905 |
| 4 | 0.995 | 1.413 | 150 | 0.99 | -21.588 |
| 5 | 0.999 | 1.413 | 151 | 1.03 | -20.159 |
| 6 | 1 | 1.413 | 201 | 1.06 | 0.000 |
| 7 | 0.99 | 1.413 | 202 | 1.045 | -5.72 |
| 8 | 1.012 | 1.413 | 205 | 1.019 | -8.359 |
| 9 | 1.003 | 1.413 | 212 | 1.06 | 1.067 |
| 10 | 0.995 | 1.413 | | | |

$B_{eq}$ for converters type #II. Therefore, both reactive power and voltage control have met the set values within the tolerance. It should be noticed that even though the voltage angle in the DC grid has a value, it remains constant though all the connected DC area. Thus, as stated earlier, there is no reactive power through the DC link, hence the DC power flow is dependent on the DC nodal voltages. The fact that the algorithm is calculating $V_a$ in the DC areas is a solid proof that the algorithm is not creating any distinction between AC and DC elements.

Simulation has converged in 5 iterations and 0.51 seconds (Processor details: Intel Core i7-6560U 2.2GHz, 16GB RAM memory, 64-bit operating system) from flat start. Meanwhile, according to the results reported in [8] employing the sequential algorithm proposed in [9], the power flow converged in 5 overall iterations. In each overall iteration, both AC grids 1 and 2 needed 4 iterations, and similarly, DC grids 1 and 2 needed 3 and 4 iterations respectively. It is also mentioned that their proposed unified method has better convergence than the sequential method. Nevertheless with the VSC model used in both [9] and [8] the power systems never present an actual interconnection. Their solution algorithms have to solve the power grid by either solving the firstly the DC grid and then the AC grid (sequential method) or creating link equations to simulate the connection (unified method). It is clear that the FGBM does create a connection between grids and therefore the effects of this interaction result in a more realistic and flexible way of simulating hybrid AC/DC power grids.

## VII. CONCLUSION

In this paper, a new steady-state FGBM model and a flexible power flow algorithm for the solution of hybrid AC/DC grids has been presented. Due to the flexibility of the FGBM, the algorithm is not creating any difference between AC, DC, or control elements. In the proposed power flow algorithm, voltage and power control is addressed per variable for all the elements, therefore several control elements of the power grid can be simulated with the same model. Simulation results demonstrate high speed quadratic convergence with full control over the grid solving AC/DC grids with pure AC methodology. This makes the model and algorithm a perfectly suitable candidate for the future development of flexible AC/DC OPF solutions. The FGBM and unified FPFA algorithm are a success.

## REFERENCES


[1] R. T. Pinto, A. C. Leon-Ramirez, M. Aragues-Penalba, A. Sumper, and E. Sorrentino, "A fast methodology for solving power flows in hybrid AC/DC networks: The european north sea supergrid case study," in *PCIM Europe 2016*, Nuremberg, Germany, May 2016.

[2] E. Bompard, G. Fulli, M. Ardelean, and M. Masera, "It's a bird it's a plane it's a...Supergrid!: Evolution opportunities and critical issues for Pan-European transmission," *IEEE Power and Energy Magazine*, vol. 12, no. 2, pp. 40–50, Feb. 2014.

[3] A. Wood, B. Wollenberg, and G. Shebl, *Power generation operation and control*, 3rd ed. New Jersey, USA: Wiley-IEEE Press, 2014.

[4] Y. Wen, J. Zhan, C. Chung, and W. Li, "Frequency Stability Enhancement of Integrated AC/VSC-MTDC Systems with Massive Infeed of Offshore Wind Generation," *IEEE Transactions on Power Systems*, pp. 1–10, Jan. 2018.

[5] W. Feng, A. L. Tuan, L. B. Tjernberg, A. Mannikoff, and A. Bergman, "A new approach for benefit evaluation of multiterminal VSCHVDC using a proposed mixed AC/DC optimal power flow," *IEEE Transactions on Power Delivery*, pp. 432–443, Jul. 2013.

[6] Z. di Wang, K.-J. Li, J. guo Ren, L.-J. Sun, J.-G. Zhao, Y.-L. Liang, W.-J. Lee, and Z. hao Ding, "A coordination control strategy of voltage-source-converter-based MTDC for offshore wind farms," *IEEE Transactions on Industry Applications*, pp. 2743–2752, Feb. 2015.

[7] J. C. F. Perez, F. M. Echavarren, and L. Rouco, "On the convergence of the sequential power flow for multiterminal VSC AC/DC systems," *IEEE Transactions on Power Systems*, vol. PP, no. 99, pp. 1–8, Jun. 2017.

[8] R. Chai, B. Zhang, J. Dou, Z. Hao, and T. Zheng, "Unified power flow algorithm based on the NR method for hybrid AC/DC grids incorporating VSCs," *IEEE Transactions on Power Systems*, vol. 31, no. 6, pp. 4310 – 4318, Nov. 2016.

[9] J. Beerten, S. Cole, and R. Belmans, "Generalized steady-state VSC MTDC model for sequential AC/DC power flow algorithms," *IEEE Transactions on Power Systems*, vol. 27, no. 2, pp. 821–829, May 2012.

[10] G. Y. Li, M. Zhou, J. He, G. K. Li, and H. F. Liang, "Power flow calculation of power systems incorporating VSC-HVDC," in *Power System Technology, 2004. PowerCon 2004*, Singapore,Singapore, Nov. 2004.

[11] J. Beerten and R. Belmans, "Development of an open source power flow software for high voltage direct current grids and hybrid ACDC systems MATACDC," *IET Generation Transmission Distribution*, vol. 9, no. 10, pp. 966 – 974, Jun. 2015.

[12] J. Beerten, D. V. Hertem, and R. Belmans, "VSC MTDC systems with a distributed DC voltage control - A power flow approach," in *PowerTech, 2011 IEEE Trondheim*, Trondheim, Norway, Sep. 2011.

[13] M. Baradar, M. Ghandhari, and D. V. Hertem, "The modeling multi-terminal VSC-HVDC in power flow calculation using unified methodology," in *Innovative Smart Grid Technologies (ISGT Europe), 2011 2nd IEEE PES International Conference and Exhibition on*, Manchester, UK, Mar. 2012.

[14] J. Lei, T. An, Z. Du, and Z. Yuan, "A general unified AC/DC power flow algorithm with MTDC," *IEEE Transactions on Power Systems*, vol. 32, no. 4, pp. 2837 – 2846, Jul. 2017.

[15] E. Acha, B. Kazemtabrizi, and L. M. Castro, "A new VSC-HVDC model for power flows using the Newton-Raphson method," *IEEE Transactions on Power Systems*, vol. 28, no. 3, pp. 2602–2612, Aug. 2013.

[16] R. D. Zimmerman, C. E. Murillo-Snchez, , and R. J. Thomas, "MATPOWER: Steady-state operations, planning and analysis tools for power systems research and education," *Power Systems, IEEE Transactions on*, vol. 26, no. 1, pp. 12–19, Feb. 2011.

[17] X.-P. Zhang, "Multiterminal voltage-sourced converter-based HVDC models for power flow analysis," *IEEE Transactions on Power Systems*, pp. 1877–1884, Nov. 2004.

[18] T. K. Vranaa, J. Beertenb, R. Belmans, and O. B. Fosso, "A classification of DC node voltage control methods for HVDC grids," *Electric Power Systems Research*, pp. 137–144, Oct. 2013.

[19] N. M. Peterson and W. S. Meyer, "Automatic adjustment of transformer and phase-shifter taps in the Newton power flow," *IEEE Transactions on Power Apparatus and Systems*, vol. 90, no. 1, pp. 103–108, Jan. 1971.

[20] W. F. Tinney, , and C. E. Hart, "Power flow solution by Newton's method," *IEEE Transactions on Power Apparatus and Systems*, vol. 86, no. 11, pp. 1449–1460, Nov. 1967.